Iranian Journal of Medical Physics

ijmp.mums.ac.ir

Monte Carlo Study of Several Concrete Shielding Materials Containing Galena and Borated Minerals

Mahdi Saeedi-Moghadam[1], Banafsheh Zeinali-Rafsanjani[1, 5], Mehdi Kazempour[2,3], Reza Jalli[1], Sedigheh Sina[4*]

[1] Medical Imaging Research Center, Shiraz University of Medical Sciences, Shiraz, Iran;
[2] MSc, Department of Radiobiology, School of paramedical sciences, Shiraz University of Medical Sciences, Shiraz, Iran;
[3] Student Research Committee, School of Paramedical Sciences, Shiraz University of Medical Sciences, Shiraz, Iran;
[4] Radiation Research Center, Shiraz University, Shiraz, Iran;
[5] Nuclear Medicine and Molecular Imaging Research Center, Shiraz University of Medical Sciences, Shiraz, Iran

ARTICLE INFO

Article type:
Original Article

Article history:
Received: Nov 04, 2016
Accepted: May 10, 2017

Keywords:
Photon
Monte Carlo
Photon Attenuation

ABSTRACT

Introduction: The heavyweight concretes have been widely used for constructing medical or industrial radiation facilities with photon sources.
Materials and Methods: In this study, heavy concretes containing galena (PbS) and several borated minerals are proposed as suitable materials against photons. The shielding properties of 21 galena concretes containing seven borated minerals with three mixing patterns were evaluated using MCNP4C Monte Carlo code. The attenuation of the gamma radiation is computed under the conditions of narrow and beam geometries. The x-ray sources with 40, 60, 90, and 120 kVp and gamma rays of ^{99m}Tc, ^{131}I, ^{137}Cs, and 511 keV annihilation photons were considered. The photon flux values and the x-ray spectrum after applying all the concretes were compared to the ordinary ones. Regarding the results, more photon attenuations obtained by using high density concretes simulation in comparison to ordinary concrete.
Results: The results revealed that the concretes containing orthopinokiolite as the borated material made by the third mixing pattern, had the most photon attenuation. According to the results, the shielding properties of the concretes containing different borated minerals were alike against high photon energies, whereas in low energy photons the attenuation depended on the type of borated mineral used in the concretes.
Conclusion: The high-density heavy-weighted concretes could be effectively used as multi-purpose shield for radiotherapy rooms and nuclear reactors due to the borated minerals.

► *Please cite this article as:*
Saeedi-moghadam M, Zeinali-Rafsanjani B, Kazempour M, jalli R, Sina S. Monte Carlo Study of Several Concrete Shielding Materials Containing Galena and Borated Minerals. Iran J Med Phys 2017; 14: 241-250. 10.22038/ijmp.2017.17873.1157.

Introduction

Nowadays imaging by ionizing radiation is one of the most powerful medical diagnosis procedures. By increasing the popularity of this method, appropriate plans for protecting the radiation workers and other people is necessary.

The concrete is one of the most commonly used shielding materials due to its acceptable mechanical properties and affordability. The concretes can be produced using diverse components and molecular structures. The aggregates play an important role in shielding properties of the concretes against different radiations such as photons and neutrons. Heavyweight concretes can be constructed using the aggregates with high specific gravity. [1-12]

The radiation attenuation properties of heavyweight concretes with the density of 2.9 to 6.0 g/cm3 produced by heavy materials and aggregates, have been widely investigated [1-12]. Bashter et al. in 2006 conducted a study on the neutron and photon shielding properties of steel scrap concrete with the density of 4 g/cm^3. It was concluded that the steel scrap concrete is more effective radiation shield in comparison to ilmenite, ilmenite–limonite, hematite–serpentine, and ordinary concrete [13].

In 2007, a heavy concrete with the density of 4.200 to 4.600 g/cm^3 was developed using galena (PbS) with half-value layer (HVL) of 2.6 cm for using against ^{60}Co gamma rays by Mortazavi et al. [14]. A heavy concrete with the density of 4.420 to 4.650 g/cm^3 using galena and datolite minerals was produced for shielding nuclear facilities and radiotherapy rooms in 2010 [15]. The HVL thickness of the datolite-based concrete samples for ^{60}Co gamma rays was found to be 2.56 cm, which was much less than that of ordinary concrete. Another heavyweight concrete was also developed by this

*Corresponding Author: Radiation Research Center, Shiraz University, Shiraz, Iran. Tel: 09172228349, 07132334033, Fax: +987136473035, Email: samirasina@yahoo.com; samirasina@shirazu.ac.ir

group using colemanite as the borated mineral and galena, with the density of 4.100 to 4.650 g/cm^3 and HVL thickness of 2.49 cm for ^{60}Co gamma rays [16]. It was showed that the neutron absorption of the heavyweight concrete was 10% greater than the reference concrete.

An intermediate-weight concrete was also developed by Aghamiri et al. in 2012, using ulexite and galena with the density of 3.640 to 3.900 g/cm^3, and HVL thickness of 2.87 cm for ^{60}Co gamma rays and a very significant improvement in neutron absorption [15].

A new generation of heavyweight concretes was introduced by Dem'yanova et al. in 2014, using the byproducts of the glass industry. They proposed the optical glass based heavyweight concrete as an effective aggregator in radiation facilities [17].

Several investigations have been conducted on attenuation properties of heavyweight concretes containing different minerals like datolite [14], ulexite [15], optical glass [17], barite [17, 19], galena, hematite–serpentite, ilmenite–limonite, basalt–magnetite, ilmenite, magnetite, basalt [2], and steel scrapes [20].

Monte Carlo simulation has been confirmed as a strong tool in assessing the attenuation properties of different radiation shields [21, 22]. In 2015, Kazempour et al. designed new combinations of non-lead radiation shields ((W-Si), (W-Sn-Ba-EPVC), and (W-Sn-Cd-EPVC)) using Monte Carlo simulations. The results of their Monte Carlo simulations demonstrated that the proposed non-lead shields were effective for 60 to 120 kVp x-ray energies [21].

In 2015, Zehtabian et al. simulated multi-layered lead-free shields for protection against photons in diagnostic radiology and nuclear medicine using MCNP5 Monte Carlo code. A three-layered shield composed of tungsten, bismuth, and gadolinium was proposed as an appropriate substitute for lead shields [22].

Multi-purpose concretes containing borated minerals might be effectively used in mixed photon and neutron beams in nuclear facilities, research, and medical centers. This study aimed to design several borated heavyweight concretes for applying in mixed radiation fields. For this purpose, a comprehensive study executed to investigate the photon attenuation properties of several multi-purpose high density concretes containing borated minerals using MCNP4c Monte Carlo code.

Materials and Methods

Different heavy weight and borated materials were offered for multi-purpose concretes construction, applicable for photon shielding. Seven types of borated minerals, such as colemanite, hydroboracite, priceite, ulexite, datolite, orthopinakiolite, and tourmaline were suggested with three mixing patterns to construct a total of 21 concretes. The mixing patterns contained 56.3%, 61.3%, and 66.3% galena.

The density and mixing patterns of different minerals are shown in tables 1 and 2, respectively.

Table 1. The density of minerals for concretes

	Material	Chemical formula	Density (ρ) (g/cm^3)
Minerals	Cement	----	3.131
	Micro Silica	----	2.1
	Galena	PbS	7.6
Borated mineral	Ulexite	$NaCa[B_5O_6(OH)_6].5H_2O$	1.96
	Datolite	$CaBSiO_4(OH)$	2.9
	Colemanite	$Ca_2B_6O_{11}•5(H_2O)$	2.42
	Hydroboracite	$CaMgB_6O_8(OH)_6•3(H_2O)$	2.17
	Priceite	$Ca_2B_5O_7(OH)_5•H_2O$	2.70
	Orthopinakiolite	$(Mg,Mn^{++})_2Mn^{+++}BO_5$	3.97
	Tourmaline	$(Na,Ca)_3B_3Al_6Si_6O_{27}(OH,F)_4$	3.3

Table 2. Three mixing patterns considered for concretes

	First mixing pattern (Weight %)	Second mixing pattern (Weight %)	Third mixing pattern (Weight %)
Galena	56.3%	61.3%	66.3%
Borated minerals (See table 1)	20%	15%	10%
Cement	17%	17%	17%
Water	5%	5%	5%
Micro silica	1.7%	1.7%	1.7%
Water to cement ratio	0.4%	0.4%	0.4%

The densities of the concretes in the first mixing pattern are 3.49, 3.67, 3.72, 3.8, 3.84, 3.92, and 4.24 g/cm^3 for ulexite, hydroboracite, colemanite, priceite, datolite, tourmaline, and orthopinakiolite, respectively. These values are 3.73, 3.89, 3.92, 3.96, 4.026, 4.09, and 4.34 g/cm^3 for the second mixing pattern. The concretes developed by the third mixing pattern using 66% galena have the maximum densities which are 4.01, 4.12, 4.15, 4.20, 4.23, 4.27, and 4.456 g/cm^3 for ulexite, hydroboracite, colemanite, priceite, datolite, tourmaline, and orthopinakiolite, respectively.

The concretes with the density of 3.49 to 4.46 g/cm^3 designed in this study were considerably denser than the ordinary concrete and comparable with those designed in previous investigations [1-16]. The photon attenuation properties of all 21 concretes were checked using MCNP4C Monte Carlo code for different photon energies in radiology and nuclear medicine.

MCNP4C Monte Carlo simulations

MCNP4C modeling, a general-purpose Monte Carlo transport code has been used in this study. This code can consider different radiation interactions such as photoelectric absorption, scattering, and pair production [23]. This code uses ENDF/B VL8 cross section library.

Two geometries including broad and narrow beams were modeled in this study, like the geometries used by Kazempour et al. in 2015 [21]. The concrete slab with a dimension of 0.1×10×10 cm^3 was placed near the uncollimated detector in broad beam geometry. The detector was not collimated to be in reach of the scattered radiation. According to the geometry used by McCaffrey et al. in 2012, in the simulation of narrow beam geometry, the source and the detector were well-collimated and the cubical slabs of each concrete were located between them [24]. The distance between the source and detector was 50 cm.

Along with the previous studies, all the simulations were performed for only one thickness, since this study aimed to compare the attenuation of photons by different materials, not to estimate the HVL. The x-ray sources with kVps of 40, 60, 90, and 120, and the gamma rays emitted from ^{99m}TC, ^{131}I, and ^{137}Cs, and 511 kev annihilation photons have been studied in this investigation. The x-ray spectra were obtained using the IPEM 78 spectrum generating software [25]. The F4 and F5 Tallies were used to score the photon flux after applying the concrete.

The energy spectra after applying the shields were calculated using F5 tally, the point detector and employing tally energy card (En). The spectra after using all the shields were normalized related to the spectrum after the shield with the least attenuation, which indicated the greatest x ray flux. All simulations were performed on 10^9 particles, in order to ensure that more than five percent were reached. No variance reduction technique was used in this study.

The photon attenuation properties ($\frac{I}{I_0}$) of the designed high density concretes with 1 mm thickness for both narrow and broad beam geometries were obtained by the tally F4 of the Monte Carlo simulation. Tally F4 is designed to compute the number of the particle track lengths per unit volume, which is the fundamental definition of flux. The 'I' value is the photon flux after applying 1 mm concrete and I_0 value is the photon flux in absence of any shields. The values of $\frac{I_{OC}}{I_C}$, the relative values of the flux after using the ordinary (I_{OC}) and the heavy concretes (I_C), were also obtained.

The validation of MCNP results, conducted by obtaining the HVL of lead for narrow beam geometry and comparing to the real value. To discover the HVL of the lead, the flux after applying (20 cm×20 cm) lead sheets with different thicknesses (0.1 cm to 1.5 cm) was attained using tally F4, and the HVL was found as the thickness of lead, after which the flux of photons reduced to the half of its initial value.

Results

To validate the MCNP simulations, the computed HVL of lead against ^{60}Co gamma rays was compared to the real HVL. Regarding the results, the HVL of lead was found to be 1.25 cm, which was comparable to its real value which was about 1.24 cm. The largest flux value for 40 kVp x-ray was observed after applying the hydroboracite concrete mixed by the first pattern (hydroboracite_1). The maximum flux value after using hydroboracite_1 was normalized to 1, and all other values were relatively changed.

The normalized spectra are shown in Figure 1, which indicate that the third mixing pattern had better attenuation properties than the others due to containing more galena. The comparison of the x-ray spectrum after using the ordinary concrete with two designed concretes using hydroboracite_1 and tourmaline_3 is demonestaed in Figure 2 . As it is obviously showed in this figure, the 40 kVp photon attenuation caused by the designed concretes is significantly higher than the ordinary concrete.

The analogy between the photon attenuation properties ($\frac{I}{I_0}$) of the designed high density concretes with 1 mm thickness and both narrow and broad beam geometries for 40 kVp x-rays and the $\frac{I_{OC}}{I_C}$ values are presented in Table 3. As these results indicated, the designed concretes could be effectively used for radiation shielding against low energy photons.

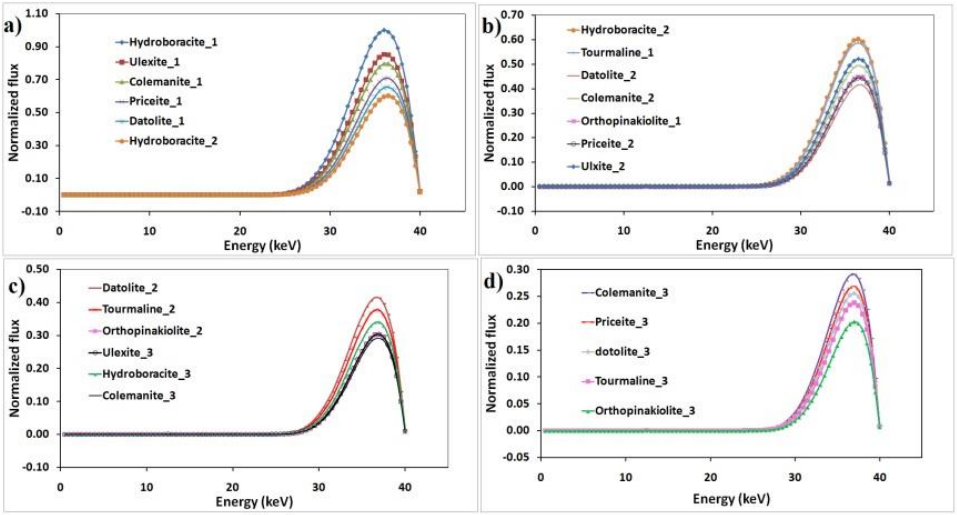

Figure 1. The comparison of the normalized x-ray spectra after using the shield for all 21 concretes.
** Ulexite_1, Ulexite_2, and Ulexite_3 introduce the concretes containing Ulexite, made by the first, second, and third mixing patterns, respectively.

Table 1. Relative transmission $(\frac{I}{I_0})$, and $(\frac{I_{OC}}{I_C})$, and , for 1mm of different concretes for 40 kvp

	$(\frac{I}{I_0})$ Narrow beam geometry	$(\frac{I}{I_0})$ Broad beam geometry	$(\frac{I_{OC}}{I_C})$ Narrow beam geometry	$(\frac{I_{OC}}{I_C})$ Broad beam geometry
Hydroboracite_1	0.0088	0.0095	47.39	44.44
Ulexite_1	0.0074	0.0080	56.50	52.91
Colemanite_1	0.0068	0.0074	61.35	57.14
Priceite_1	0.006	0.0065	69.44	64.94
Datolite_1	0.0054	0.0058	77.52	72.99
Hydroboracite_2	0.0049	0.0053	85.47	80.00
Tourmaline_1	0.0048	0.0051	86.96	82.64
Ulexite_2	0.0042	0.0044	99.01	96.15
Colemanite_2	0.0039	0.0042	107.53	101.01
Orthopinakiolite_1	0.0035	0.0038	119.05	111.11
Priceite_2	0.0035	0.0037	119.05	113.64
Datolite_2	0.0032	0.0034	129.87	125.00
Tourmaline _2	0.0029	0.0031	144.93	136.99
Orthopinakiolite_2	0.0023	0.0024	181.82	175.44
Ulexite_3	0.0023	0.0024	181.82	175.44
Hydroboracite_3	0.0026	0.0027	161.29	156.25
Colemanite_3	0.0022	0.0023	188.68	185.19
Priceite_3	0.002	0.0021	208.33	200.00
Datolite_3	0.0019	0.0020	217.39	212.77
Tourmaline_3	0.0017	0.0018	243.90	232.56
Orthopinakiolite_3	0.0014	0.0015	294.12	277.78
Ordinary concrete	0.4173	0.4224	1.00	1.00

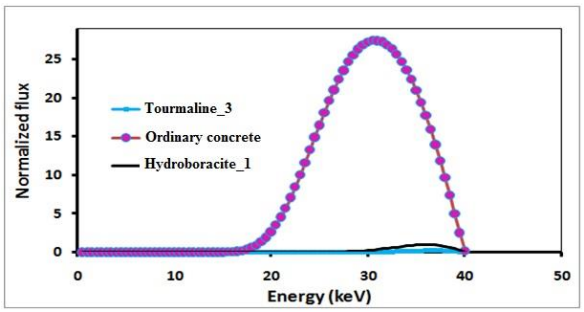

Figure 2. The comparison between the x-ray spectra after applying the ordinary concrete and two of the concretes designed in this study

The x-ray fluxes after applying all the designed concretes made by the third mixing pattern for 60 kVp x-rays, are compared and showed in Figure 3. The results signified that the concrete containing orthopinakiolite had the best attenuation in 60 kVp x-ray field. The comparison between the spectra after applying hydrobarocite_3 and ordinary concretes is exhibited in Figure 4. The analogy of the photon attenuation properties $(\frac{I}{I_0})$ for 60 kVp x-rays by applying different concretes and the $\frac{I_{OC}}{I_C}$ values are shown in Table 4. Giving to the results, the designed concretes significantly reduced the 60 kvp x-ray flux.

Table 2. Relative transmission $(\frac{I}{I_0})$, $(\frac{I_{OC}}{I_C})$, for 1mm of different concretes for 60kvp.

	$(\frac{I}{I_0})$ Narrow beam geometry	$(\frac{I}{I_0})$ Broad beam geometry	$(\frac{I_{OC}}{I_C})$ Narrow beam geometry	$(\frac{I_{OC}}{I_C})$ Broad beam geometry
Hydroboracite_1	0.0775	0.0783	7.76	7.75
Ulexite_1	0.0709	0.0743	8.49	8.17
Colemanite_1	0.0684	0.0718	8.80	8.45
Priceite_1	0.0640	0.0673	9.41	9.02
Datolite_1	0.0612	0.0645	9.83	9.42
Hydroboracite_2	0.0585	0.0616	10.29	9.85
Tourmaline_1	0.0577	0.0608	10.43	9.99
Ulexite_2	0.0540	0.0569	11.15	10.67
Colemanite_2	0.0525	0.0553	11.47	10.98
Orthopinakiolite_1	0.0500	0.0432	12.03	14.04
Priceite_2	0.0495	0.0523	12.17	11.61
Datolite_2	0.0478	0.0645	12.59	9.42
Tourmaline _2	0.0454	0.0481	13.26	12.63
Orthopinakiolite_2	0.0405	0.0427	14.86	14.22
Ulexite_3	0.0404	0.0431	14.90	14.08
Hydroboracite_3	0.0430	0.0458	14.01	13.26
Colemanite_3	0.0395	0.0422	15.24	14.39
Priceite_3	0.0378	0.0430	15.92	14.12
Datolite_3	0.0368	0.0374	16.37	16.23
Tourmaline_3	0.0354	0.0380	17.01	15.97
Orthopinakiolite_3	0.0326	0.0350	18.45	17.33
Ordinary concrete	0.6019	0.6071	1.00	1.00

Table 3. Relative transmission $(\frac{I}{I_0})$, $(\frac{I_{OC}}{I_C})$, for 1mm of different concretes for 90kvp.

	$(\frac{I}{I_0})$ Narrow beam geometry	$(\frac{I}{I_0})$ Broad beam geometry	$(\frac{I_{OC}}{I_C})$ Narrow beam geometry	$(\frac{I_{OC}}{I_C})$ Broad beam geometry
Hydroboracite_1	0.29	0.30	2.72	2.67
Ulexite_1	0.28	0.29	2.82	2.76
Colemanite_1	0.27	0.28	2.93	2.86
Priceite_1	0.26	0.27	3.04	2.96
Datolite_1	0.26	0.27	3.04	2.96
Hydroboracite_2	0.25	0.26	3.16	3.08
Tourmaline_1	0.25	0.26	3.16	3.08
Ulexite_2	0.24	0.25	3.29	3.20
Colemanite_2	0.24	0.25	3.29	3.20
Orthopinakiolite_1	0.23	0.24	3.44	3.33
Priceite_2	0.23	0.24	3.44	3.33
Datolite_2	0.23	0.24	3.44	3.33
Tourmaline _2	0.22	0.23	3.59	3.48
Orthopinakiolite_2	0.21	0.22	3.76	3.64
Ulexite_3	0.21	0.22	3.76	3.64
Hydroboracite_3	0.22	0.23	3.59	3.48
Colemanite_3	0.21	0.22	3.76	3.64
Priceite_3	0.20	0.21	3.95	3.81
Datolite_3	0.20	0.21	3.95	3.81
Tourmaline_3	0.20	0.21	3.95	3.81
Orthopinakiolite_3	0.19	0.20	4.16	4.00
Ordinary concrete	0.79	0.80	1.00	1.00

The x-ray spectrum after applying one of the high-density concretes like hydroboracite_3 was compared with this spectrum after applying the ordinary concrete and the spectrum without any shield for 90 kVp x-rays (Figure 5). As mentioned before, the third mixing pattern had higher photon attenuation than the others; The x-ray spectrum after applying them is shown in Figure 6.

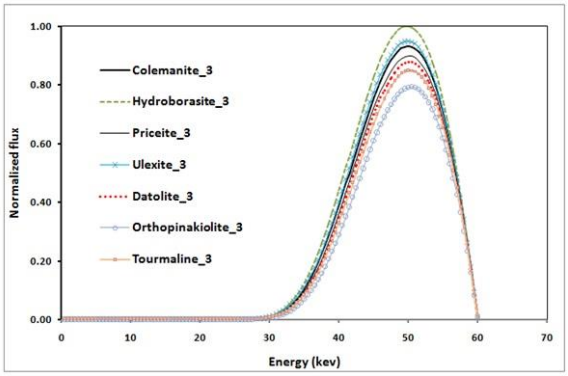

Figure 3. The comparison of the energy spectra after applying the high density concrete made by third mixing pattern for 60 kVp x-rays.

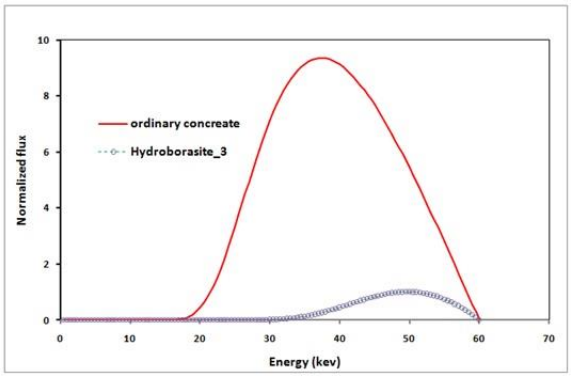

Figure 4. The comparison of the energy spectra after applying hydroboracite_3 and ordinary concrete for 60 kVp x-rays.

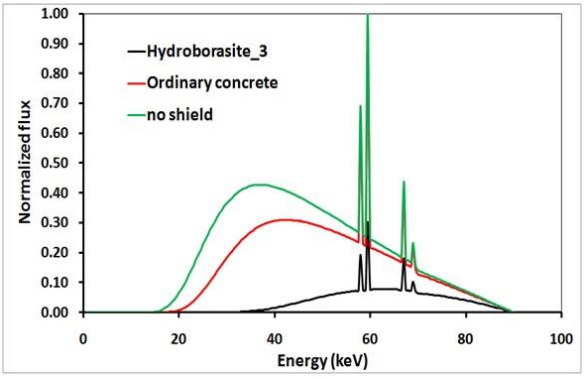

Figure 5. The comparison between the energy spectra after applying the hydrobarosite_3 and ordinary concretes for 90 kVp x-rays.

The photon attenuation properties ($\frac{I}{I_0}$) for 90 kVp x-rays is demonstrated in Table 5. The obtained results revealed that the designed high density concretes could reduce the x-ray fluence more than the ordinary concrete. The comparison of the x-ray spectrum after administering hydrobarocite_3 shield with the x-ray spectrum after ordinary concrete is shown in Figure 7. The normalized spectra for 120 kVp x-rays after using the concretes made by third mixing pattern are displayed in Figure 8. According to the figures, after applying all the designed concretes, an immediate reduction was observed at 90 keV which was equal to the K-edge energy of lead presented in galena (PbS).

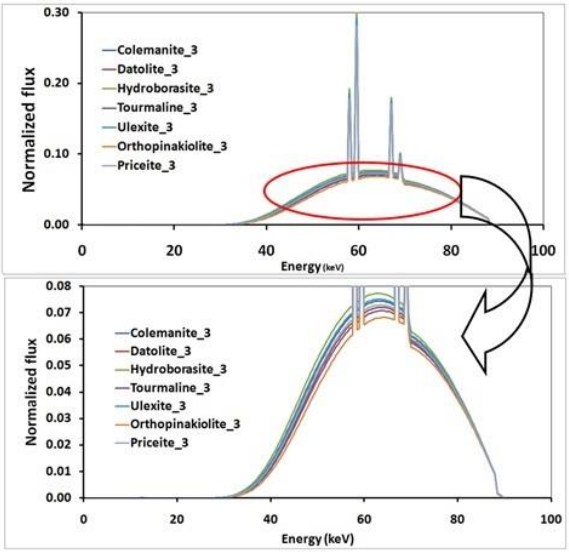

Figure 6. The comparison between the energy spectra after using high density concrete and the concretes mixed by third pattern for 90 kVp x-rays.

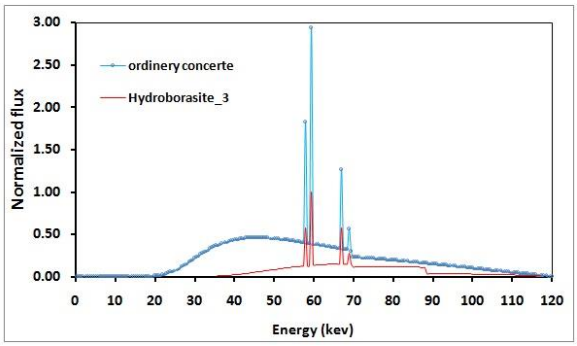

Figure 7. The comparison between the energy spectra after using the hydrobarocite_3 and ordinary concretes for 120 kVp x-rays.

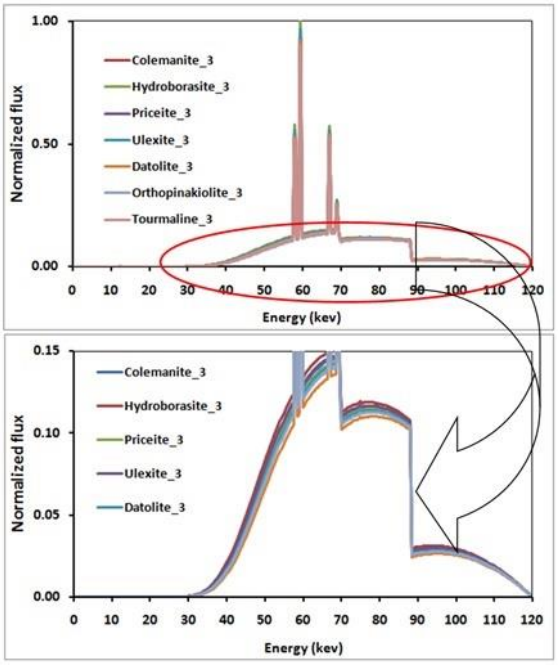

Figure 8. The comparison between the energy spectra after applying the high density concrete and the concretes mixed by the third pattern for 120 kVp x-rays.

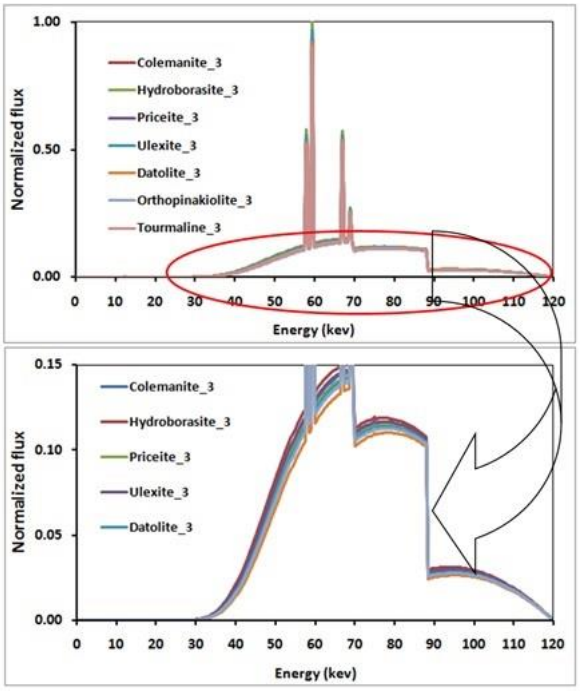

Figure 9. (a) The $\frac{I}{I_0}$ value for the concretes mixed by the first pattern (b) The $\frac{I}{I_0}$ value for the concretes mixed by second pattern (c) The $\frac{I}{I_0}$ value for the concretes mixed by third pattern (d) The $\frac{I}{I_0}$ value for the concretes containing orthopinakiolite made by three mixing patterns.

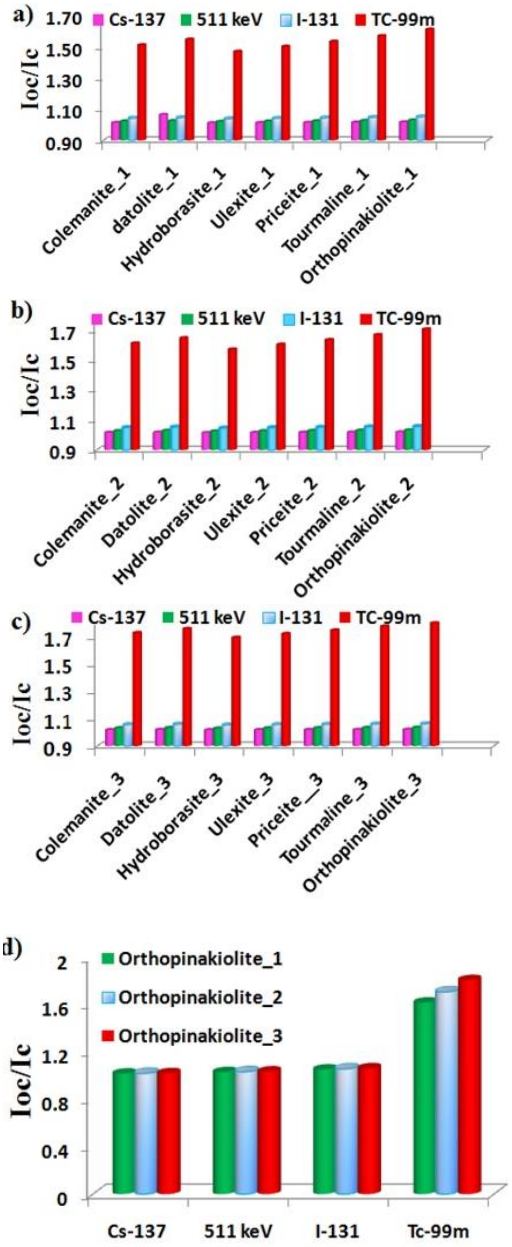

Figure 10. The comparison between the photon fluxes after applying ordinary concrete and a) the concretes mixed by the first pattern b) the concretes mixed by second pattern c) the concretes mixed by third pattern d) the concretes containing orthopinakiolite made by three mixing patterns.

The photon attenuation properties ($\frac{I}{I_0}$) for 120 kVp x-rays is presented in Table 6. Regarding the results, the designed concretes could be effectively used for radiation shielding against low energy photons. The gamma ray attenuation, produced by different concretes were compared and demonstrated in figures 9 and 10.

Table 4. Relative transmission $(\frac{I}{I_0})$,$(\frac{I_{OC}}{I_C})$ for 1mm of different concretes for 120kvp.

	$(\frac{I}{I_0})$ Narrow beam geometry	$(\frac{I}{I_0})$ Broad beam geometry	$(\frac{I_{OC}}{I_C})$ Narrow beam geometry	$(\frac{I_{OC}}{I_C})$ Broad beam geometry
Hydroboracite_1	0.221	0.230	3.31	3.20
Ulexite_1	0.210	0.219	3.48	3.36
Colemanite_1	0.206	0.214	3.55	3.44
Priceite_1	0.198	0.207	3.69	3.56
Datolite_1	0.194	0.202	3.77	3.65
Hydroboracite_2	0.189	0.197	3.87	3.74
Tourmaline_1	0.187	0.195	3.91	3.78
Ulexite_2	0.181	0.189	4.04	3.90
Colemanite_2	0.178	0.189	4.11	3.90
Orthopinakiolite_1	0.173	0.181	4.22	4.07
Priceite_2	0.172	0.180	4.25	4.10
Datolite_2	0.169	0.176	4.33	4.19
Tourmaline _2	0.164	0.172	4.46	4.28
Orthopinakiolite_2	0.154	0.161	4.75	4.58
Ulexite_3	0.154	0.161	4.75	4.58
Hydroboracite_3	0.160	0.167	4.57	4.41
Colemanite_3	0.152	0.159	4.81	4.64
Priceite_3	0.149	0.155	4.91	4.76
Datolite_3	0.149	0.153	4.91	4.82
Tourmaline_3	0.144	0.151	5.08	4.88
Orthopinakiolite_3	0.137	0.144	5.34	5.12
Ordinary concrete	0.731	0.737	1.00	1.00

Discussion

As it is obviously concluded that the photon flux after applying an ordinary concrete with the thickness of 1 mm was about 294 times more than heavy concrete containing orthopinakiolite made by third mixing pattern (orthopinakiolite_3) for 40 kVp x-ray (Table 3). The best attenuation between all heavy concretes was observed in orthopinakiolite_3 shielding, since the photoelectric is the predominant effect in 40 kVp energy range, and the attenuation of the photons depends significantly on the effective atomic number.

The results of the simulations for 60 kVp x-rays, revealed that orthopinakiolite_3 had the best attenuation between all the heavy concretes, as orthopinakiolite is the heaviest discovered borated mineral . The value of $\frac{I_{OC}}{I_C}$ for narrow beam geometry was found to be 18.45 for orthopinakiolite_3, which demonstrated the 18.45 times more attenuation after applying 1 mm Orthopinakiolite_3 in comparison to the ordinary concrete with the same thickness.

The comparison of $\frac{I_{OC}}{I_C}$ for 90 and 120 kVp x-rays showed the reduction of the x-ray fluence from 18.74% to 28.73% and 24.05% to 35.44% of the fluence by using the designed high density concretes in comparison to the ordinary concrete, respectively.

As demonestrated in tables 4 and 5, by increment of the energy, the attenuation properties of heavy concretes have been reduced. This is due to the domination of the photoelectric effect in low energy x-rays and the importance of the atomic number in photon attenuation. However, as the photon energy increased, the probability of the compton effect increased, and it led to the photon attenuation coefficients decrement.

The results of this study indicated that the heavy concretes were very effective for using as shield in the low-energy x-ray facilities, while for higher energy photons of ^{131}I, ^{137}Cs, and annihilation photons there were no significant differences between the photon flux after applying the high density concretes and the ordinary ones.

Figures 9a and 9c presented the comparison between the fluxes after using the heavy concretes and in absence of the shields. The results indicated that the flux values after applying heavy concretes with the thickness of 1 mm for ^{99m}Tc gamma rays were reduced from 60% to 96% of the flux values, when no shield was applied. Slight improvement in photon attenuation was observed using heavy concretes compared to the ordinary one, for higher energy photons of ^{131}I, ^{137}Cs, and the annihilation photons (Figure 9). As presented in Figure 9d, although identical attenuations observed for high energy photons emitted from ^{131}I, ^{137}Cs, and 511 kev photons, but different attenuations were detectable for 140 kev photons of ^{99m}Tc by applying the concretes constructed by the noted mixing patterns in both groups.

The comparison between the fluxes after ordinary concrete and those after applying the heavy concretes made by the first, second, and the last mixing patterns are shown in figures 10a to 10c. The results indicated that the fluxes after using ordinary concrete, (I_{oc}), for ^{99m}Tc gamma rays was 1.52 to 1.81

times more than the fluxes after applying our heavy concretes. According to figure 10d, for such high energy photons, the concretes constructed by the mixing patterns demonstrated approximately equal attenuations, while for 140 keV gamma rays of ^{99m}Tc the photon, the flux after administering the heavy concretes containing Orthopinakiolite with the mixing patterns, it was 55% to 62% of the fluxes after using the ordinary ones.

The analogy between this study results with the literature review [17, 23], showed that the (I/I_0) values raised significantly by increasing the kVp of the photons from 40 kV to 120 kV for different combinations of materials In shield construction.

Therefore, it could be concluded that the heavy concretes could be effectively utilized in construction of the medical imaging rooms. Furthermore, the borated concretes are suggested to be used as shielding structures in the mixed radiation fields containing both photons and neutrons.

It worth to be mentioned that the simulated shields in this study were assumed to be completely homogeneous, while it was impossible to make a completely homogeneous shield.

Conclusion

The designed high-density concretes seems to be effectively used as multi-purpose concretes for shielding radiotherapy rooms and nuclear reactors due to the borated minerals. The construction of radiation facilities using such borated heavy concretes enabled us to utilize different kinds of equipment in the designed buildings, without need to add more borated, and heavy shields. Supplementary investigations are recommended to optimize the percentage of borated minerals in different neutron fields.

References

1. Bashter, II. Neutron relaxation lengths in light and heavy concrete shields. 1993.
2. Bashter, II, Abdo AE-S, Abdel-Azim MS. Magnetite ores with steel or basalt for concrete radiation shielding. Japanese journal of applied physics. 1997;36(6R):3692. DOI: 10.1143/JJAP.36.3692.
3. Akkurt I, Akyildirim H, Mavi B, Kilincarslan S, Basyigit C. Gamma-ray shielding properties of concrete including barite at different energies. Progress in Nuclear Energy. 2010;52(7):620-3. DOI: 10.1016/j.pnucene.2010.04.006.
4. Akkurt I, Akyıldırım H, Mavi B, Kilincarslan S, Basyigit C. Radiation shielding of concrete containing zeolite. Radiation Measurements. 2010;45(7):827-30. DOI: 10.1016/j.radmeas.2010.04.012.
5. Akkurt I, Akyıldırım H, Mavi B, Kilincarslan S, Basyigit C. Photon attenuation coefficients of concrete includes barite in different rate. Annals of Nuclear Energy. 2010;37(7):910-4. DOI: 10.1016/j.anucene.2010.04.001
6. Akkurt I, Basyigit C, Kilincarslan S, Mavi B, Akkurt A. Radiation shielding of concretes containing different aggregates. Cement and Concrete Composites. 2006;28(2):153-7. DOI: 10.1016/j.cemconcomp.2005.09.006.
7. Akkurt I, Baysigit C, Kilincarslan S, Beycioglu A. Prediction of photon attenuation coefficients of heavy concrete by fuzzy logic. Journal of the Franklin Institute. 2010;347(9):1589-97. DOI: 10.1016/j.jfranklin.2010.06.002.
8. Demir F, Budak G, Sahin R, Karabulut A, Oltulu M, Un A. Determination of radiation attenuation coefficients of heavyweight-and normal-weight concretes containing colemanite and barite for 0.663 MeV γ-rays. Annals of Nuclear Energy. 2013; 38(6):1274-8. DOI: 10.1016/j.anucene.2011.02.009.
9. Maruyama T, Kumamoto Y, Kato Y, Hashizume T, Moriyuki Y. Attenuation of 4-32 MeV X-rays in Ordinary Concrete, Heavy Concrete, Iron and Lead. Health physics. 1971;20(3):277-84. DOI: 10.1097/00004032-197103000-00005.
10. Urabe I, Kobayashi K, Fujita Y, Tsujimoto T, Guangchuan J. Depth distribution of residual radioactivities in the concrete wall of an electron linac facility. Health physics. 1991;60(4):587-91.
11. Bashter, II. Radiation attenuation and nuclear properties of high density concrete made with steel aggregates. Radiation effects and defects in solids. 1997;140(3-4):351-64. DOI: 10.1080/10420159708216859.
12. Mortazavi SMJ, Mosleh-Shirazi MA, Maheri MR, Yousefnia H, Zolghadri S, Haji-pour A. Production of an economic high-density concrete for shielding megavoltage radiotherapy rooms and nuclear reactors. Iran J Radiat Res. 2007;5(3):143-6.
13. Mortazavi SMJ, Mosleh-Shirazi MA, Roshan-Shomal P, Raadpey N, Baradaran-Ghahfarokhi M. High-performance heavy concrete as a multi-purpose shield. Radiation protection dosimetry. 2010 Oct 29;142(2-4):120-4.. DOI: 10.1093/rpd/ncq265.
14. Mortazavi SMJ, Mosleh-Shirazi MA, Baradaran-Ghahfarokhi M, Siavashpour Z, Farshadi A, Ghafoori M, et al. Production of a datolite-based heavy concrete for shielding nuclear reactors and megavoltage radiotherapy rooms. Iran J Radiat Res. 2010; 8(1):11-5.
15. Aghamiri SMR, Mortazavi SMJ, Razi Z, Mosleh-Shirazi MA, Baradaran-Ghahfarokhi M, Rahmani F, et al. Ulexite-galena intermediate-weight concrete as a novel design for overcoming space and weight limitations in the construction of efficient shields against neutrons and photons. Radiation protection dosimetry. 2013;154(3):375-80. DOI: 10.1093/rpd/ncs249.
16. Abdo AE-S, Kansouh WA, Megahid RM. Investigation of radiation attenuation properties for baryte concrete. Japanese journal of applied physics. 2002;41(12R):7512. DOI: 10.1143/JJAP.41.7512.
17. Dem'yanova VS, Kalashnikov DV. Heavy Optical Glass in Concrete for Radiation Protection. Glass and ceramics. 2014;70(9-10):338-9. DOI: 10.1007/s10717-014-9576-3.

18. Akkurt I, Basyigit C, Kilincarslan S, Mavi B. The shielding of g-rays by concretes produced with barite. Progress in Nuclear Energy. 2005;46(1):1-11. DOI: 10.1143/JJAP.41.7512.
19. Bashter, II. Calculation of radiation attenuation coefficients for shielding concretes. Annals of nuclear Energy. 1997;24(17):1389-401. DOI: 10.1016/S0306-4549(97)00003-0.
20. Bashter, II. Radiation attenuation and nuclear properties of high density concrete made with steel aggregates. Radiation effects and defects in solids. 1997;140(3-4):351-64. DOI: 10.1080/10420159708216859.
21. Kazempour M, Saeedimoghadam M, Shekoohi Shooli F, Shokrpour N. Assessment of the Radiation Attenuation Properties of Several Lead Free Composites by Monte Carlo Simulation. J Biomed Phys Eng. 2015 Jun 1;5(2):67-76.
22. Zehtabian M, Piruzan E, Molaiemanesh Z, Sina S. Design of Light Multi-layered Shields for Use in Diagnostic Radiology and Nuclear Medicine via MCNP5 Monte Carlo Code. Iranian Journal of Medical Physics. 2015; 12 (3), 223-9. DOI: 10.22038/ijmp.2015.6223.
23. Briesmeister JF. MCNPTM-A general Monte Carlo N-particle transport code. Version 4C, LA-13709-M, Los Alamos National Laboratory. 2000.
24. McCaffrey JP, Tessier F, and Shen H. Radiation shielding materials and radiation scatter effects for interventional radiology (IR) physicians. Med. Phys. 2012; 39 (7), 4537-46. DOI: 10.1118/1.4730504.
25. Cranley K, Gilmore B J, Fogarty G W A, L D. Catalogue of diagnostic x-ray spectra and other data. IPEM Report No. 78; 1997.